Characterization of defects created in Cz and epitaxial Si doped with Ga or B using Laplace-DLTS

Cloud Nyamhere, P.N.K. Deenapanray, F.D. Auret and F.C. Farlow

Abstract

We have measured the electrical and annealing properties of defects created in epitaxial and Czochralski-grown Si doped with either B or Ga by electron irradiation using both conventional and Laplace deep level transient spectroscopy (L)-DLTS. With L-DLTS, we have been able to resolve several defects that cannot be resolved using conventional DLTS. L-DLTS provides a new avenue to study defect introduction rates and annealing kinetics in B- and Ga-doped Si. The isochronal annealing behaviour of the defects was also investigated.

PACS: 71.55.-i; 73.40.Sx; 73.61.CW; 78.40.Fy

Article Outline

1. Introduction

Defects that introduce deep levels in the band gap of semiconductors, and which act as efficient recombination centres, have detrimental effects on the performance of solar cells. Defects can be created in a number of ways, including (1) growth of the semiconductor, (2) processing of device using low-energy particles (e.g. plasma etching)

or high-energy particle irradiation (e.g. particle accelerators), and (3) under operating conditions. A notable example in the latter case is the degradation of the minority carrier lifetime of B-doped Cz–Si solar cells under either illumination or carrier injection due to the formation of a metastable defect involving B and O [1]. The lifetime degradation is not observed in Ga-doped Cz–Si [1]. However, few studies have investigated Ga-related defects in p-type Si, and detailed comparative studies of defect introduction rate of defects in B- or Ga-doped Cz–Si are not numerous [2] and [3].

In this paper, we demonstrate that Laplace deep level transient spectroscopy (L-DLTS) [4] and [5] provides the high resolution to study the electronic and annealing properties of among others, closely spaced discrete level defects that cannot be achieved using conventional DLTS [6]. We have used electron-irradiated B- and Ga-doped, epitaxial and Cz grown Si as examples, respectively.

2. Experimental procedure

We have used B- and Ga-doped Si with doping concentration of 1.5×10^{16} and $3.5\times10^{16}\,cm^{-3}$, respectively. After chemical cleaning (i.e. degreasing, annealing at 300 °C and dipping in dilute HF solution), circular Ti/Al Schottky diodes were fabricated through a contact mask. The samples were irradiated with 1 MeV electrons to fluences of $1.5\times10^{16}\,cm^{-2}$(B-doped) and $3.5\times10^{16}\,cm^{-2}$(Ga-doped), respectively, at room temperature. Prior to electrical characterization, ohmic contacts were formed on the rear of samples using In–Ga eutectic. Isochronal annealing was performed on the Schottky diodes in the temperature range 30–300 °C in steps of 50 °C for 20 min in Ar. The samples were then characterized by current–voltage (*I–V*), capacitance–voltage (*C–V*), conventional (*C*-) and Laplace-DLTS. The ‘signatures’ of defects (i.e. energy position in band gap relative to the valence band, E_T, and apparent capture cross-section, *a*) were determined from Arrhenius plots of $\ln(T^2/e_h)$ vs. $1000/T$, where e_h is the hole emission rate and *T* is the measurement temperature.

3. Results and discussion

In this section, we discuss the electronic and annealing properties of hole traps created in the samples by electron irradiation. First, it is enlightening to look at the defect resolution capability of Laplace over *C*-DLTS.

3.1. Conventional vs. Laplace-DLTS

The *C*-DLTS spectrum measured from an electron-irradiated Ga-doped Cz sample irradiated and annealed at 150 °C is shown in Fig. 1. The spectrum exhibits two broad peaks positioned around 112 and 190 K that arise from overlapping defect peaks. This is evidenced by the shoulders on the high-energy side of the two main peaks. On the other hand, the insets show the spectral density functions (SDF), i.e. L-DLTS spectrum (measured around the peak positions of the two broad peak). L-DLTS is clearly able to resolve the broad DLTS peaks into two groups of discrete levels. Notably, the broad peak around 112 K is resolved into three discrete defects with levels at $E_V + 0.18eV$,

$E_V + 0.17eV$, and $E_V + 0.13eV$, while the peak around 190 K is resolved into two discrete defects with levels at $E_V + 0.37eV$ and $E_V + 0.33eV$. In each inset, the peak at the lowest emission rate is an artifact of the algorithm used to extract the SDF from measured capacitance transients at constant temperature.

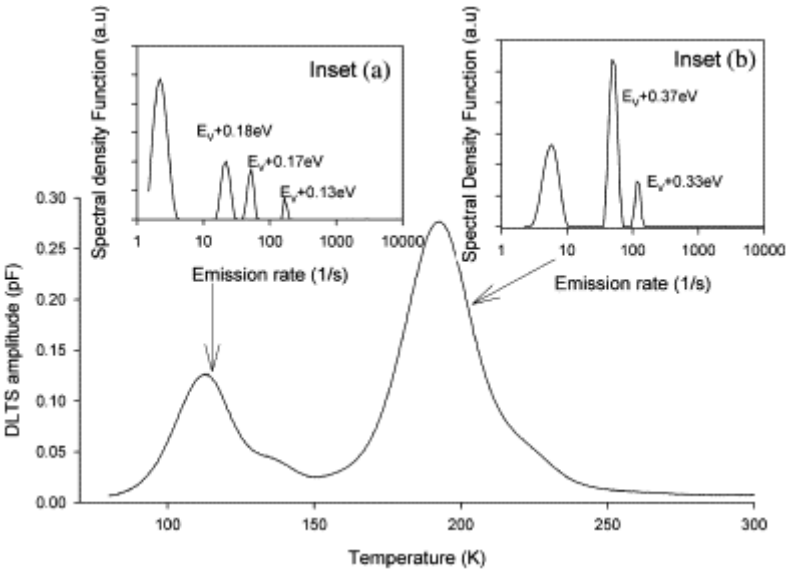

Fig. 1. *C*-DLTS spectrum from electron irradiated Ga-doped Cz–Si annealed at 150 °C.

3.2. Electronic properties of defects

We have determined the 'signature' of electron-irradiation-induced defects in B- or Ga-doped Si using Arrhenius plots of $\ln(T^2/e_h)$ vs. $1000/T$. Fig. 2 shows the plots for defects observed in the electron-irradiated B-doped sample. The 'signatures' of defects created by irradiation in B- and Ga-doped samples are summarized in Tables 1 and 2, respectively. The tables provide a comparison between the energy positions of the defects as determined by both *C*- and L-DLTS. The last column of each table indicates the structure of the defects, where the question mark sign (i.e. '?') refers to only a tentative assignment.

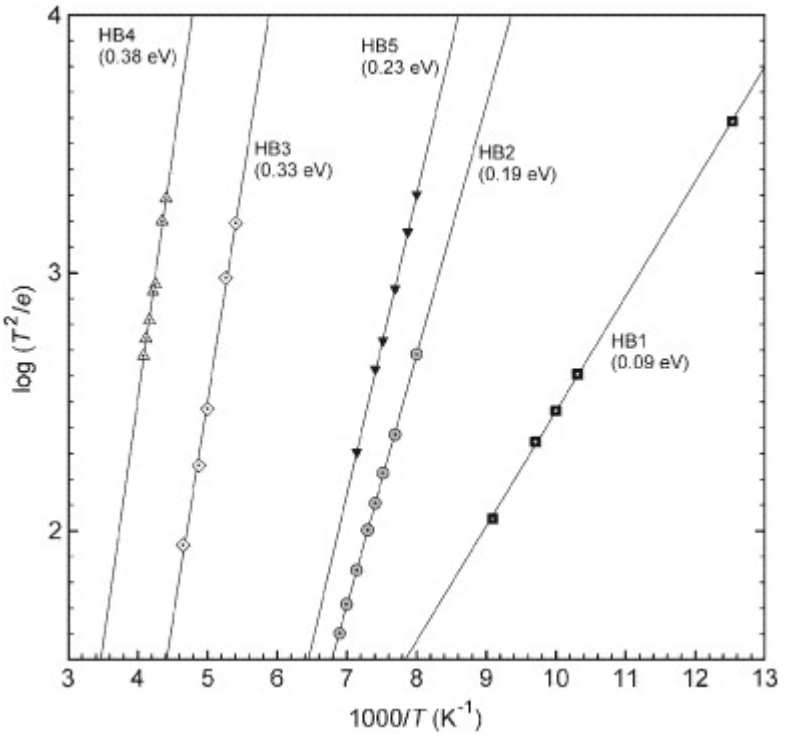

Fig. 2. An Arrhenius plot for radiation induced defects in B-doped Si.

Table 1.

Signature of defects in B-doped epitaxial Si

Defect	E_T (eV) ***C*-DLTS**	E_T (eV) **L-DLTS**	a (cm^2)	**Defect structure**
HB1	—	0.09	3.7×10^{-20}	—
HB2	0.20	0.19	3.2×10^{-17}	V–V [7]
HB3	0.29	0.33	3.3×10^{-16}	C_i–O_i [8]
HB4	0.35	0.38	3.7×10^{-20}	—
HB5	—	0.23	2.7×10^{-16}	—

Table 2.

Signature of defects in Ga-doped Cz–Si

Defect	E_T (eV) *C*-DLTS	E_T (eV) L-DLTS	a (cm^2)	Defect structure
HG1_1	0.06	0.08	4.4×10^{-20}	—
HG1_2	0.13	0.11	2.6×10^{-21}	—
HG2_1	0.13	0.14	5.1×10^{-19}	—
HG2_2	0.23	0.17	5.4×10^{-21}	—
HG2_3	—	0.18	1.1×10^{-19}	? [2] and [3]
HG3_1	0.23	0.22	1.4×10^{-19}	V–V [7]
HG3_2	0.31	0.34	3.3×10^{-16}	—
HG5	—	0.37	7.8×10^{-16}	C_i–O_i [8]
HG4	0.56	0.45	7.7×10^{-15}	V–? [6]

HB1, HB2 and HB3 are primary defects that are created during electron irradiation, and HB2 and HB3 can be attributed to the divacancy (V–V) [7] and the C_i–O_i complex respectively [8]. HB4 and HB5 are secondary defects that are detected only after the irradiated samples have been annealed at 100 °C. Secondary defects are generally created by the agglomeration of primary defects and/or constituents thereof that become mobile at higher temperatures. *C*-DLTS was unable to measure the ‘signatures’ of HB1 and HB5 in B-doped epitaxial Si.

The electronic properties of defects created in Ga-doped Cz–Si by electron irradiation were also determined by Arrhenius plots (not shown). They are summarized in Table 2.

A comparison between Tables 1 and 2 shows that a more extensive set of defects is introduced in Ga-doped sample. HG2_3 is observed only after annealing at 150 °C and more will be said about this defect later.

3.3. Annealing behaviour of defects in B-doped epitaxial Si

From a practical perspective, the complete characterization of defects requires that the annealing kinetics of the defects is established. Annealing experiments serve to determine, amongst others, (1) the temperature range within which a defect can be removed after its initial introduction, (2) whether secondary defects that may be detrimental to device performance are introduced during high-temperature steps in the

processing of devices, and (3) the structure of defects through comparative studies. For instance, the electronic ‘signatures’ of HG2_3 and HG3_1 may be similar, whereas their annealing behaviours are quite different. This subtle difference provides a versatile way to distinguish between them.

Fig. 3 shows the isochronal annealing behaviour of defects in electron-irradiated B-doped epitaxial Si. Not shown is HB5 that was introduced after annealing at 100 °C but was removed after annealing at 160 °C. The peak defect intensity was measured from spectra taken by *C*-DLTS.

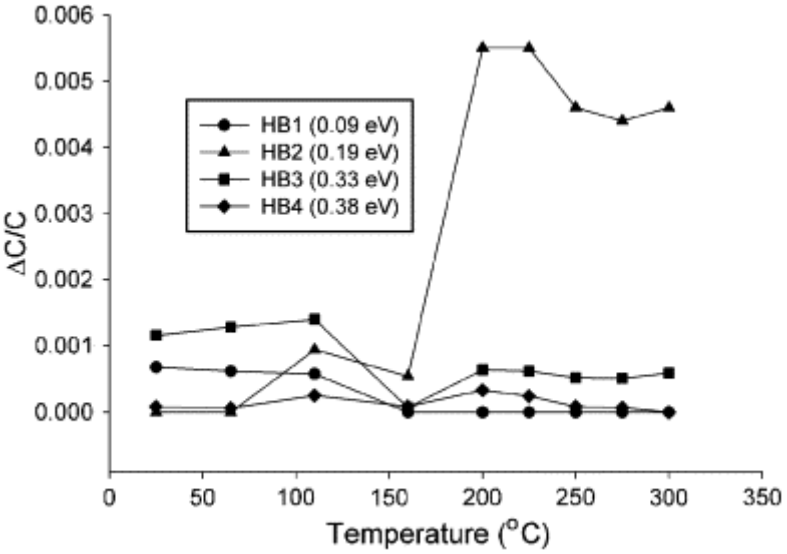

Fig. 3. Isochronal annealing behaviour of defects in electron-irradiated B-doped epitaxial Si.

The secondary defect HB4 is introduced above 100 °C and it is completely removed at 300 °C. HB3 (C_i–O_i) showed an initial decrease around 160 °C and thereafter underwent some reverse annealing. It was stable at the highest annealing temperature used in this study. A similar defect in [3] has been shown to exhibit reverse annealing properties, albeit at the higher temperature of 225 °C, in proton-irradiated samples [9]. The C_i–O_i complex is known to be thermally stable up to 350 °C in electron- or proton-irradiated samples [10]. HB1 that is thermally stable up to 160 °C only has not previously been reported, most probably because of the lack of high-resolution DLTS. This defect could only be detected in our samples following L-DLTS measurements around the peak of HB2 observed with *C*-DLTS. The most pertinent observation from Fig. 3 concerns the annealing behaviour of HB2. Fig. 3 shows that the intensity of HB2, identified here as the divacancy, increased above 160 °C, i.e. reverse annealing effect. V–V is known to be annealed out at 300 °C in electron-irradiated B-doped Cz–Si without exhibiting any reverse annealing effect [10]. In heavy proton-irradiated Cz–Si, the divacancy exhibited reverse annealing between 270 and 325 °C [9]. The difference between the reverse annealing temperature reported here and in Ref. [9] for V–V could be due to the use of

different bombardment species, sample type and fluences used in the two investigations. Since HB2 is vacancy-related, the results shown in Fig. 3 suggest that there must be a release of vacancies from other sources around 160 °C. There are two possible ways in which HB2 could grow. Single vacancies produced upon the dissociation of a complex could then agglomerate to form V–V. Alternatively, a defect complex such as V–V–*X* (*X* is an impurity), which releases V–V directly upon dissociation. A deeper understanding of the exact mechanism contributing to the growth of HB2 is not clear to us at present, since this will require measurement of defects in the upper half of the band gap. Such measurements are currently underway as part of our initiative to determine the detailed annealing kinetics of defects in B- or Ga-doped Si.

3.4. Annealing behaviour of defects in Ga-doped Cz–Si

We now turn to the isochronal annealing behaviour of the hole traps observed in electron-irradiated Ga-doped Cz–Si. For convenience, like in the case of B-doped Si, the spectra obtained using *C*-DLTS were used to monitor the annealing behaviour of defects. Fig. 4 depicts the change in the peak intensity of the defects as a function of annealing temperature.

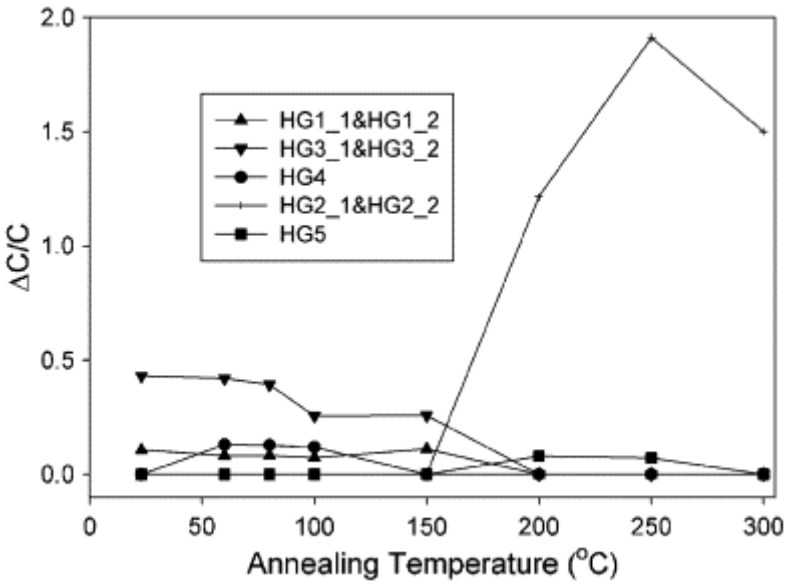

Fig. 4. Isochronal annealing behaviour of defects in electron-irradiated Ga-doped Cz–Si.

There are a few notable differences between the annealing behaviour of defects in Ga-doped compared to B-doped epitaxial Si. The most pertinent one regards the behaviour of V–V that does not exhibit the reverse annealing effect. This suggests one of two scenarios, namely (1) that the source of vacancies present in B-doped Si is not present in Ga-doped Cz–Si, and/or (2) the release of vacancies, if this source were present, is preferentially scavenged by impurities like interstitial oxygen or oxygen dimmers. Regarding the latter situation, it has been suggested that the formation of Ga_i–O_i defect is

inhibited in Ga-doped Cz–Si, which may imply a larger reservoir of interstitial oxygen to complex with vacancies released during annealing. Once, again one would have to monitor the annealing behaviour of the V–O centre $(E_C - 0.18\,eV)$ to clarify this point. Another difference is the absence of C_i–O_i in the as-irradiated Ga-doped Cz–Si. In fact, C_i–O_i is only observed after annealing at 200 °C. This clearly reveals that the formation of this complex is inhibited in Ga-doped Cz–Si, and is consistent with results previously reported in Refs. [2] and [3].

Finally, the combination HG2_1 and HG2_2 is introduced by annealing at 150 °C and, although it was still stable at 300 °C, its intensity was on the decrease. A defect with energy position at 0.18 eV relative to the valence band and displaying identical annealing behaviour has previously been reported in electron-irradiated Ga-doped Cz–Si. This defect has been suggested to be a complex involving Ga_i [2].

4. Summary

We have studied the electronic and annealing properties of defects created in B-doped epitaxial Si- and Ga-doped Cz–Si by 1 MeV electron irradiation. In particular, we have shown that the better resolution of L-DLTS over *C*-DLTS provides a new way for the detailed characterization of defects in p-type Si. It has been shown that in B-doped epitaxial Si, the divacancy grows during annealing above 160 °C. In contrast, the divacancy did not display the reverse annealing effect in Ga-doped Cz–Si. There are other features of defect introduction and their annealing in Ga-doped Cz–Si that are consistent with results previously reported in the literature. Our results reveal that further investigation has yet to be carried out on Ga-doped Cz–Si in order to provide a complete picture of the properties of defects created in this material. We are currently measuring the detailed annealing kinetics of defects, as well as correlating the introduction rates of defects and free carrier compensation in the electron-irradiated samples using L-DLTS.

References

[1] J. Schmidt and K. Bothe, *Phys. Rev. B* **69** (2004), p. 024107.

[2] A. Khan, M. Yamaguchi, Y. Ohshita, N. Dharmarasu, K. Araki, T. Abe, H. Itoh, T. Ohshima, M. Imaizumi and S. Matsuda, *J. Appl. Phys.* **90** (2001), p. 1170.

[3] M. Yamaguchi, A. Khan, T.K. Vu, Y. Ohshota and T. Abe, *Physica B* **340–342** (2003), p. 596.

[4] L. Dobaczewski, P. Kaczor, I.D. Hawkins and A.R. Peaker, *J. Appl. Phys.* **76** (1994), p. 194.

[5] L. Dobaczewski, A.R. Peaker and K.B. Nielsen, *J. Appl. Phys.* **96** (2004), p. 4689.

[6] F.D. Auret and P.N.K. Deenapanray, *Crit. Rev. Solid State Mater. Sci.* **29** (2004), p. 1.

[7] F. Volpi, A.R. Peaker, I. Berbezier and A. Ronda, *J. Appl. Phys.* **95** (2004), p. 4752.

[8] G.L. Miller, D. Lang and L.C. Kimerling, *Ann. Rev. Mater. Sci.* **7** (1977), p. 377.

[9] A. Khan, M. Yamaguchi, T. Hisamatsu and S. Matsuda, *J. Appl. Phys.* **87** (2000), p. 2162.

[10] P.M. Mooney, L.J. Cheng, M. Süli, J.D. Gerson and J.W. Corbett, *Phys. Rev. B* **8** (1977), p. 3836.